Grid turbulence in solid body rotation

P. Orlandi

EUROMECH Colloquium 525, 21–23 June 2011, Écully, France
Instabilities and transition in three-dimensional flows with rotation

GRID TURBULENCE IN SOLID BODY ROTATION

Presenting P. Orlandi,
Dipartimento di Ingegneria Meccanica e Aerospaziale
Università La Sapienza, Via Eudossiana 16, I-00184, Roma

1 Introduction

Isotropic turbulence is generated in wind tunnels by an uniform stream going through a solid grid. After an anisotropic region the flow becomes isotropic, and decays in the streamwise direction with a power law $(x_1/M)^{-m}$. In a laboratory it is rather difficult to investigate the effects of the solid body rotation on the power law decay. The study is easier in numerical experiments with three periodic directions and a synthetic isotropic turbulence at $t = 0$ which decays as t^{-m}. The power law m changes with the rotation number $N = 2\Omega L/U$, the inverse of the Rossby number used in geophysical flows. In this setup the initial conditions are different from those in real experiments. However in the experiments even the grid rotates and therefore the inlet conditions may change with the rotation rate.

In the present study the Navier-Stokes equations in a rotating frame are solved in a domain with dimensions $12\pi \times 2\pi \times 2\pi$ respectively in the streamwise, and in the other two homogeneous directions. Radiative boundary conditions at $L_1 = 12\pi$ allow the disturbance to exit from the computational domain. At the inlet an analytical velocity distribution $U_l = \delta_{1l} + A_l \sin(fx_2)\sin(fx_3) + A_R(x_2, x_3)$ is assigned, with $A_1 = 0$, $A_2 = A_3 = 0.25$ and $A_R = 0.01$. The solidity of the grid is $M = 2\pi/f$. This inlet condition is not isotropic having a turbulent stress $\langle u_2 u_3 \rangle \neq 0$ which should go to zero at a distance x_1/M to have an isotropic turbulent flow, further downstream decreasing as $(x_1/M)^{-m}$. The simulations are performed at a Reynolds number, which, for non rotating conditions close to the exit, has $R_\lambda = O(10)$ and $m = 2.5$. Several simulations were performed with fixed $f = 8$ and N varying from 1 to 10. Note that these values correspond to rotation rates higher than those achieved in laboratory experiments (Jacquin *et al.*[1]).

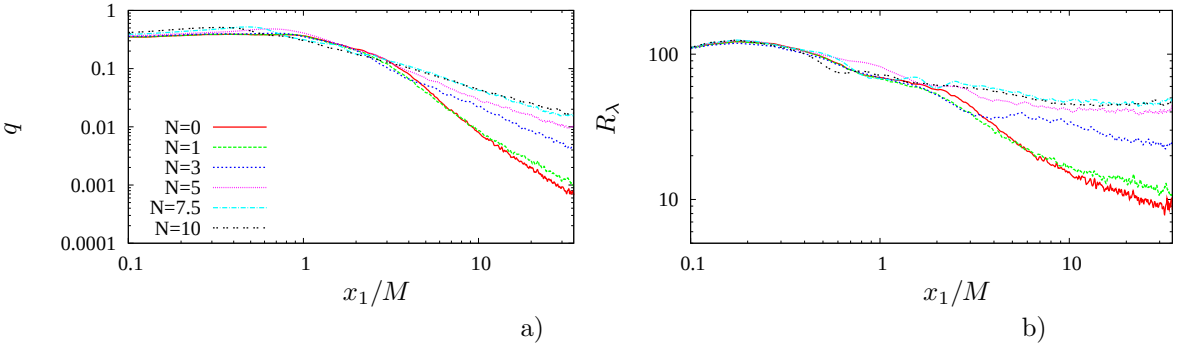

Figure 1: Profiles of a) q and b) R_λ versus x_1/M at different values of N.

Preliminary simulations show a large reduction of m with N (Fig.1a). The streamwise oscillations of q, not so evident in this figure because of the log scale, in a normal scale show a decrease of the amplitude and an increase of the wave length with the increase of N . This is an evidence that the vortical structures become longer when N raises. This effect has been recently observed in rotating tank experiments by Moisy *et al.*[2] where the turbulence is generated at $t = 0$ and then decays in time. Here the conditions are different being the small scales generated at the inlet, and survive together with those downstream which are modified by the rotation. The additional effect of rotation is to reduce the energy transfer from large to small scales and therefore the rate of energy dissipation. This is demonstrated by the streamwise evolution of R_λ in Fig.1 where, at high N, R_λ is constant ($m \approx 1$).

To understand in more detail the streamwise evolution across the anisotropic and isotropic regions it is worth looking at the u_1 equation in rotational form, where the kinetic energy q appears together with the components of the Lamb vector ($\lambda = \mathbf{v} \times \omega$), related to the energy transfer from large to small scales

$$\frac{\partial q}{\partial x_1} - \langle u_2\omega_3 \rangle + \langle u_3\omega_2 \rangle = -\frac{\partial \langle p \rangle}{\partial x_1} = \frac{\partial \langle u_1^2 \rangle}{\partial x_1} \tag{1}$$

In this equation the direct effect of N does not enter, which instead acts on the other two velocity components modifying $\lambda_\mathbf{1}$. To understand the effects of N on the streamwise evolution of the velocity rms $\langle u_l^2 \rangle$, which for $N = 10$ are compared in Fig.2a with those for $N = 0$. For $N = 0$ $\langle u_1^2 \rangle$ grows for the positive contribution

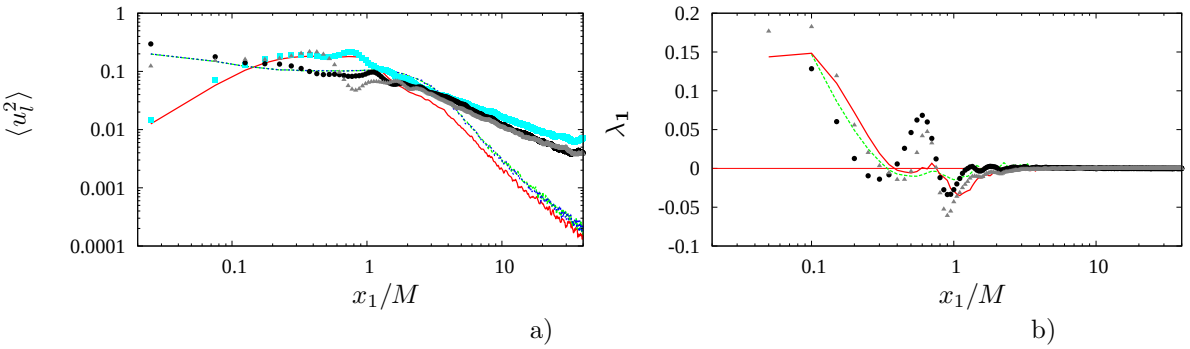

Figure 2: Profiles of a) the velocity rms (——— , ■, $l = 1$ - - - - , ● , $l = 2$ ····· , ▲, $l = 3$ and b) the component λ_1 (- - - - , ■) and $\frac{\partial \langle p \rangle}{\partial x_1}$ (——— , ▲) versus x_1/M; lines $N = 0$, solid symbols $N = 10$. ———

of the λ_1 component (Fig.2b), and the other two equal stresses decrease in x_1. At the end of the anisotropic region ($x_1/M \approx 3$) all the stresses decrease, although $\langle u_1^2 \rangle$ is slightly smaller than the other two. The transport equations for $\langle u_l^2 \rangle$ ($l \neq 1$) stresses show a positive contribution of N for one and negative for the other, this is visible in Fig.2a, where, for $N = 10$ in the anisotropic region, $\langle u_2^2 \rangle$ and $\langle u_3^2 \rangle$ are different. Through this imbalance a greater $\langle u_1^2 \rangle$ than that for $N = 0$ is obtained. The cause is visible in Fig.2b where positive values of λ_1 occur in correspondence of the $\langle u_1^2 \rangle$ bump.

By increasing the solid body rotation the helicity density $h = \mathbf{v} \cdot \omega$ increases, which from the identity $|\mathbf{v} \times \omega|^2 + |\mathbf{v} \cdot \omega|^2 = |\mathbf{v}|^2 |\omega|^2$ reduces the transfer from large to small scales, and the energy remains at the large scales. The helicity distribution is zero in the non-rotating case and grows with the rotation rate, with a positive contribution up to $x_1/M \approx 1$ and negative downstream. The analysis of the Lamb vector and the helicity density will be presented in more detail at the conference. The transfer of energy to the large scales, characteristic of rotating flows, can be observed by the spectra together with streamwise vorticity visualizations at the same location. In particular at $x_1/M = 2$ and at $X_1/M = 10$ the transverse spectrum $E_{33}(k_2)$, for all values of N, and, for $N = 0$ and $N = 10$, contour plots of $\omega_1(x_2, x_3)$ are considered. The spectra in Fig.3a together with the ω_1 contours in Fig.3b show that the influence of the inlet disturbance at $x_1/M = 2$ is large for $N = 0$ and that it reduces by increasing N. In Fig.3c, at high N, the inlet disturbances are less visible, while larger structures appear. The spectra show better the transfer of energy to large scales. At $x_1/M = 10$ the figures 3d-f clearly demonstrate the formation of energetic large scales at $N = 10$, which are those giving $m = 1$.

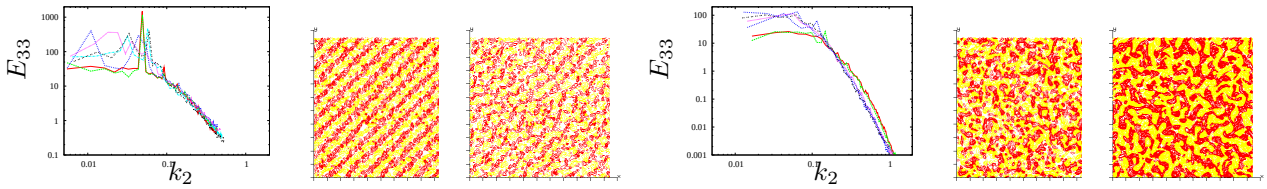

Figure 3: Transverse spectra, a) $x_1/M = 2$, d) $x_1/M = 10$ different N lines as Fig.1; contours plot of ω_1 b) for $N = 0$ c) $N = 10$ at $x_1/M = 2$ with $\Delta\omega_1 = 1$ e) for $N = 0$ f) $N = 10$ at $x_1/M = 10$ with $\Delta\omega_1 = 0.1$

References

[1] L., Jacquin, O., Leuchter, C., Cambon, & J., Mathieu Homogeneous turbulence in the presence of rotation. *J. Fluid Mech.* **220**, 1–52 (1990)

[2] F., Moisy , C., Morize , M., Rabaud & J., Sommeria Decay laws, anisotropy and cycloneanticyclone asymmetry in decaying rotating turbulence *J. Fluid Mech.* **666**, 5–35 (2011)